Electronic Supplementary Material (ESI) for Journal of Materials Chemistry C.

SUPPORTING INFORMATION

Ionic Interactions Control the Modulus and Mechanical Properties of Molecular Ionic Composite Electrolytes

Joshua E. Bostwick,[1] Curt J. Zanelotti,[2] Deyang Yu,[2] Nicholas F. Pietra,[2] Teague A. Williams,[3] Louis A. Madsen,[2]* and Ralph H. Colby[1]*

[1]*Department of Materials Science and Engineering, Pennsylvania State University, University Park, Pennsylvania 16802, United States*

[2]*Department of Chemistry and Macromolecules Innovation Institute, Virginia Tech, Blacksburg, Virginia 24061, United States*

[3]*Materials Research Institute, Pennsylvania State University, University Park, Pennsylvania 16802, United States*

AUTHOR INFORMATION

Corresponding Authors

Email*: lmadsen@vt.edu, rhc@plmsc.psu.edu

Ionic Liquid Molecular Volume Determination

The molecular volumes (V_m) of the IL were determined through

$$V_m = \frac{mN_{av}}{\rho} \quad \textbf{(S1)}$$

where m is the molar mass of the IL, ρ is the density of the IL and N_{av} is Avogadro's number.

The mass and density of the ILs were provided from their respective vendor and values of V_m are listed in **Table S1**.

Table S1: Ionic liquid (IL) densities (ρ) at a specified temperature (listed in the technical data sheet provided by the vendor) and molecular volumes (V_m) used in this study. These values were determined through **Eq. (S1)**.

Ionic Liquid	Density (ρ) (g cm^{-3})	Molecular Volume (V_m) (nm^3)
BMIm-DCA	1.06 (25 °C)	0.322
EMIm-TfO	1.39 (25 °C)	0.311
BMIm-TfO	1.30 (24 °C)	0.368
EMIm-TFSI	1.52 (20 °C)	0.427
BMIm-TFSI	1.44 (19 °C)	0.484
BMPyr-TFSI	1.40 (23 °C)	0.501

Determination of Shear Storage Modulus

To get proper comparisons between the tensile and storage moduli in the MICs, we employed linear viscoelastic analysis under shear. **Figure S1** shows the strain dependence of the shear storage modulus (*G*') of the MICs at a fixed frequency of 1 rad s^{-1} at 30 °C. In each of the MICs, two trends are shown in *G*': a near strain-independent plateau at low strains and a strain-dependent decrease at high strains. These two regions represent the linear and nonlinear viscoelastic regions of strain respectively and the linear region is used to make proper comparisons with the Young's modulus found in the MICs.[1]

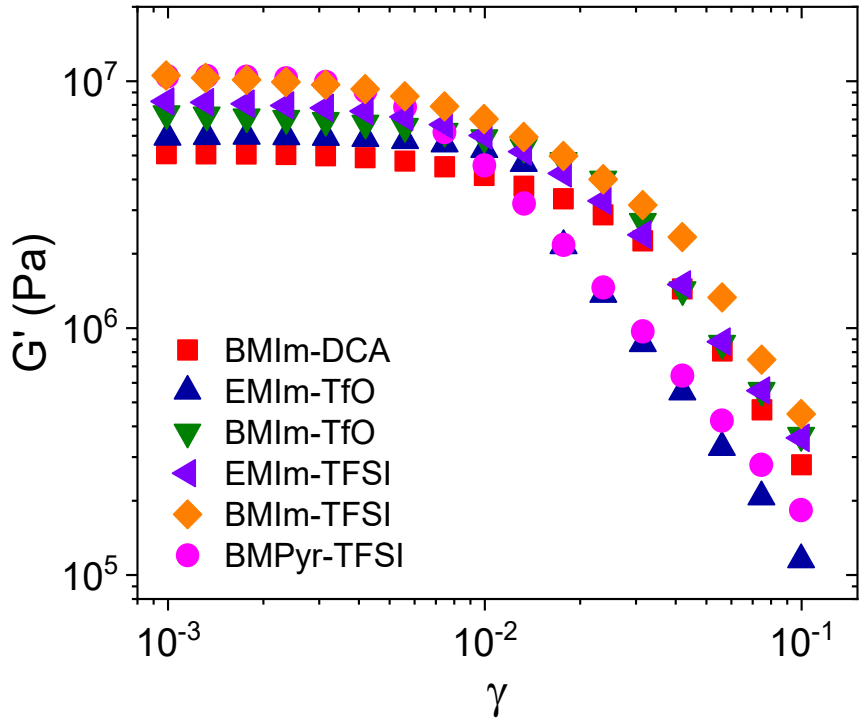

Figure S1: Strain amplitude of the shear storage modulus (*G*') for the 10 wt% PBDT MICs at a frequency of 1 rad s^{-1} at 30 °C using 3 mm diameter parallel plates. *G*' was taken in the low strain limit signifying the linear viscoelastic response. The shear thinning slope is roughly -1.7, suggesting that the MICs delaminate from the plates at high strain amplitude.

DSC Traces of Neat Ionic Liquids and Molecular Ionic Composites

Figure S2a and **Figure S2b** shows the DSC traces of the ILs and MICs, respectively using a TA Instruments DSC 2500. All samples were loaded into aluminum hermetic pans with a sample mass between 6 – 10 mg. All of the ILs undergo crystallization and melting shown by their respective exothermic and endothermic peaks. However, once the IL is combined with the PBDT, crystallization is not seen at all in the 10 K min^{-1} heating rate for the ILs with $TFSI^-$ anions and crystallization is far smaller for the other three ILs. The strong ionic interactions of cations with the PBDT suppresses crystallization.[2]

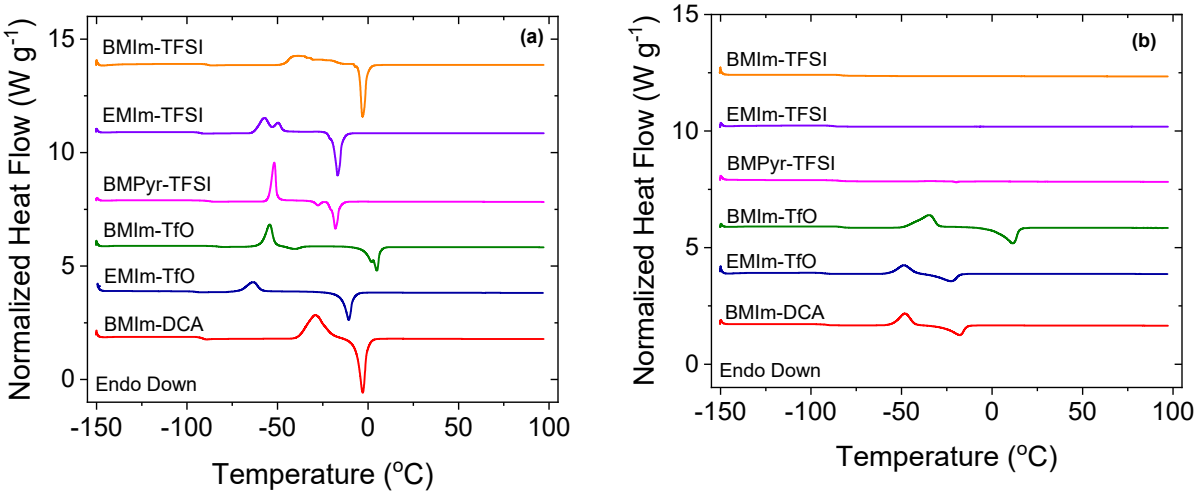

Figure S2: DSC curves (endo down) of the **(a)** ILs and **(b)** MICs with 10 wt% PBDT at a heating rate of 10 K min^{-1} after cooling at 10 K min^{-1} (second scans) up to 100 °C. T_g was determined as the midpoint of the change in heat capacity.

Dielectric Relaxations in ILs and MICs

In order to evaluate the ion dynamics through DRS, the out-of-phase part of permittivity (ε") is commonly evaluated to determine the relaxation processes. However, as shown in **Figure S3a** as filled symbols (for the BMIm-DCA IL and MIC at –65 °C), the ionic conductivity contribution of ε" outweighs the relaxation contribution and results in the relaxation being masked.[3, 4] Therefore, we evaluated the relaxation process in both the ILs and the MICs through their derivative spectra (ε_{der}).[5]

$$\varepsilon_{der} = -\frac{\pi}{2}\frac{\partial \varepsilon'(\omega)}{\partial ln\omega} \quad \textbf{(S2)}$$

Depicted in **Figure S3a** as open symbols, one clear relaxation process (α) is shown in both the BMIm-DCA IL and MIC at –65 °C. In order to determine the peak characteristic frequency related to the relaxation process (ω_{max}), ε_{der} was then fit to a power law for EP[6] and one Havriliak–Negami (HN) fit[7]

$$\varepsilon_{der} = A\omega^{-s} - \frac{\pi}{2}\left(\frac{\partial \varepsilon'_{HN}(\omega)}{\partial ln\omega}\right)_{\alpha} \quad \textbf{(S3)}$$

$$\text{with } \varepsilon'_{HN}(\omega) = Real\left\{\frac{\Delta\varepsilon}{\left[1+\left(\frac{i\omega}{\omega_{HN}}\right)^{\beta}\right]^{\gamma}}\right\}$$

where A and s are constants, $\Delta\varepsilon$ is the dielectric strength of the relaxation, β and γ are shape parameters related to the HN fit, and ω_{HN} is a characteristic frequency related to ω_{max} through

$$\omega_{max} = \omega_{HN}\sin\left(\frac{\beta\pi}{2+2\gamma}\right)^{1/\beta}\sin\left(\frac{\beta\gamma\pi}{2+2\gamma}\right)^{1/\beta} \quad \textbf{(S4)}$$

In all of the ILs and MICs measured, we saw one clear α relaxation process over a wide temperature range and this α relaxation occurs at longer times in the MIC relative to the IL. We suspect this is

due to the IL ions interacting with the sulfonate groups in the PBDT-IL bundle phase, slowing down the diffusive motion of charge carriers and lowering the overall ionic conductivity relative to their neat IL. Due to the decreased motion of the charge carriers in the MIC, we hypothesize that the DRS α relaxation of MICs corresponds to the rearrangement of IL ions during charge transport[8, 9] both from the IL-puddle phase and the PBDT-IL bundle phase ($\omega_{max} = \omega_{\alpha}$). This idea of a single α relaxation in MICs was shown from a previous study where an α relaxation process was probed through linear viscoelastic measurements.[10]

Shown in **Figure S3b**, the ω_{max} peak in the α relaxation for the ILs and MICs is fit with the VFT equation,

$$\omega_{max} = \omega_{\infty} \exp\left(-\frac{BT_0}{T - T_0}\right) \quad \textbf{(S5)}$$

where ω_{∞} is the relaxation frequency at infinite temperature, B is a dimensionless parameter reciprocally related to fragility and T_0 is the Vogel temperature determined from the VFT fit to the ionic conductivity with parameters listed in **Table S2**. Incorporating the ILs into the PBDT matrix showed a decrease in ω_{max}, indicative of slower diffusive motion of charge carriers and an increase in T_g. To relate the ion rearrangement of the ILs and MICs with the thermal T_g determined from DSC, we extrapolated the VFT fits down to 10^{-2} rad s^{-1} (100 s). This corresponds to the dynamic T_g from DRS.[11] The T_g from DRS and T_g from DSC are in good agreement with one another for both the ILs and MICs, with all T_g differences from the two characterization techniques ranging between 0 – 5 $^{\circ}$C. This illustrates that the α relaxation from DRS corresponds to the dynamics of the IL glass transition over the entire frequency range.

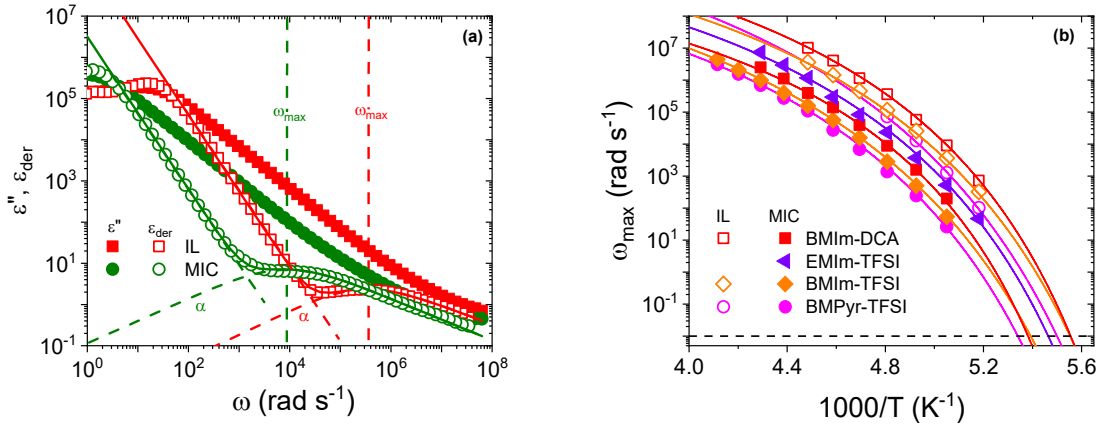

Figure S3: (a) Imaginary permittivity (ε", filled) and its derivative (ε_{der}, open) at –65 °C for the BMIm-DCA IL and its respective 10 wt% PBDT MIC. Both the IL and MIC curves are fit to derivative spectra (solid line) using a combination of one HN fit (dashed line) and a power law to EP (dashed line). The spectra reveal one α relaxation and the peak in this relaxation is the reciprocal of the characteristic relaxation time (ω_{max}) in both the ILs and MICs. **(b)** Temperature-dependent ω_{max} of ILs and MIC films. Data were fit to the VFT equation with parameters listed in **Table S2** and fixed to the same Vogel temperature as the ionic conductivity. Fits were extrapolated down to 10^{-2} rad s^{-1} (100 s, dashed line) to give the dynamic glass transition temperature (T_g) in DRS listed in **Table S2** with comparisons to the DSC T_g.

Table S2: Fitting parameters from the VFT temperature-dependence (**Eq. S4**) of dielectric relaxation for both the ILs and MICs. Glass transition temperature comparisons between the DSC and DRS characterization techniques.

	IL					MIC				
Sample	log ω_∞ (rad s^{-1})	B	T_0 (K)	DRS T_g (K)	DSC T_g (K)	log ω_∞ (rad s^{-1})	B	T_0 (K)	DRS T_g (K)	DSC T_g (K)
BMIm-DCA	12.3	5.3	155	180	181	10.7	4.5	161	186	181
EMIm-TFSI[a]	N/A	N/A	N/A	N/A	180	11.7	5.7	155	183	185
BMIm-TFSI	12.1	6.0	152	180	185	11.5	6.6	153	185	190
BMPyr-TFSI	12.9	7.0	151	181	186	11.2	6.1	156	187	189
[a]DRS T_g of EMIm-TFSI IL was not determined due to IL crystallization on cooling.										

VFT Fits of the Ionic Conductivity

Table S3: Fitting parameters from the VFT temperature dependence (**Eq. (2)**) of the ionic conductivity and DSC T_g.

	IL				MIC			
Sample	σ_∞ (S cm^{-1})	B	T_0 (K)	DSC T_g (K)	σ_∞ (S cm^{-1})	B	T_0 (K)	DSC T_g (K)
BMIm-DCA	1.62	5.0	155	181	0.62	4.5	161	181
EMIm-TfO	0.87	4.3	154	178	1.05	5.9	145	180
BMIm-TfO[a]	N/A	N/A	N/A	N/A	N/A	N/A	N/A	N/A
EMIm-TFSI	2.69	6.3	146	180	1.15	5.6	155	185
BMIm-TFSI	2.00	6.0	152	185	1.32	6.6	153	190
BMPyr-TFSI	2.40	6.6	151	186	0.72	6.0	156	189
[a]BMIm-TfO IL and MIC VFT fits are not listed due to crystallization preventing measurement at low enough temperatures.								

Normalized Room Temperature Ionic Conductivity

We analyzed the differences between the ionic conductivity (σ_o) of the IL and its corresponding 10 wt% PBDT MIC through **Figure S4** where the ionic conductivity of the MIC (σ_{MIC}) is normalized by the ionic conductivity of the IL (σ_{IL}) at 30 °C. All MICs maintain an ionic conductivity within roughly a factor of 3 with their respective IL most likely due to the MICs containing a volume fraction of approximately 50% IL puddles where the IL moves like the neat IL.

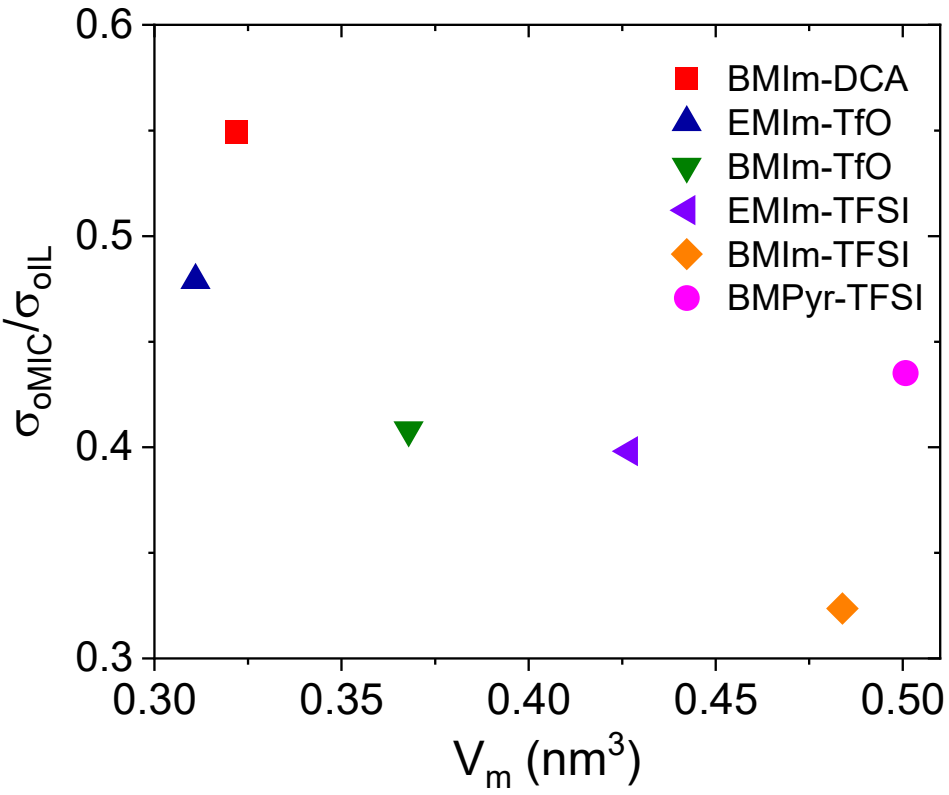

Figure S4: Normalized MIC ionic conductivity (σ_{MIC}/σ_{IL}) plotted against the Il molecular volume (V_m) at 30 °C.

Molar Conductivity of MICs

The molar conductivity (Λ_o) of the MICs were determined through

$$\Lambda_o = \frac{\sigma_{MIC} m}{\rho} \quad \textbf{(S6)}$$

where σ_{MIC} is the ionic conductivity of the MIC, m is the mass of the IL and, ρ is the density of the neat IL listed in **Table S1**. **Figure S5** shows the Λ_o plotted against V_m in the MICs. All MICs with an ethyl chain cation produced higher Λ_o compared to the MICs with the same anion but with larger cation size, in part because the latter has a smaller number density of charge carriers.

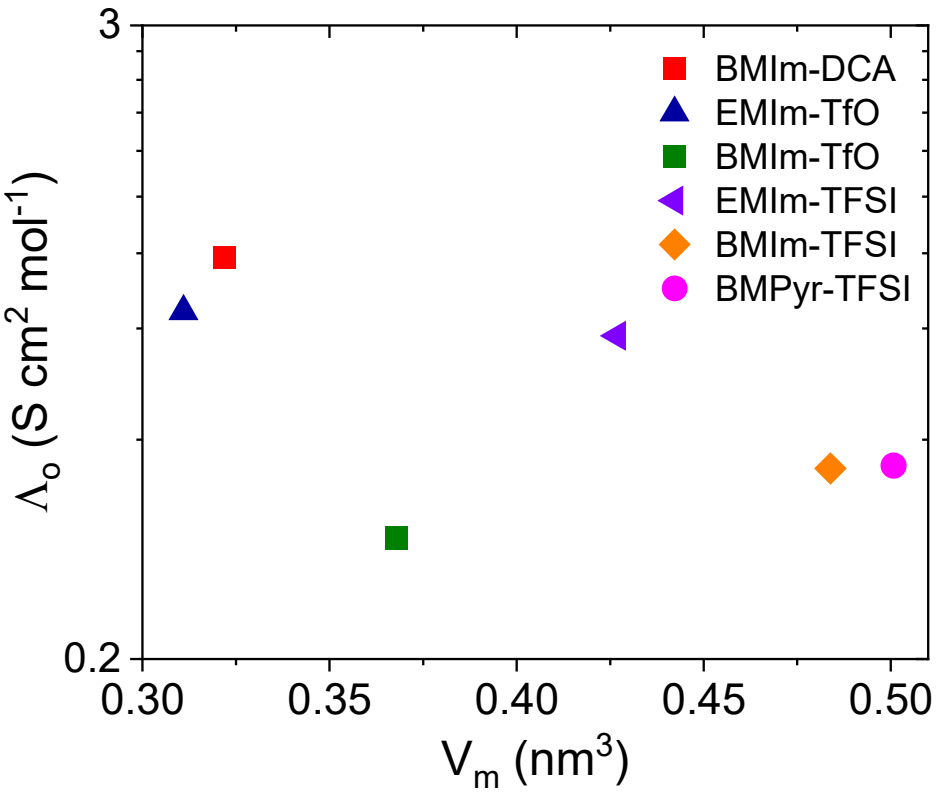

Figure S5: Molar conductivity (Λ_o) plotted against IL V_m at 30 °C. Increasing the IL alkyl chain length decreased Λ_o in similar IL anion MICs causing smaller alkyl chain MICs to produce higher ionic conductivities.

VFT Fits of the Ionic Diffusion

Table S4: Fitting parameters from the VFT temperature dependence (**Eq. (7)**) for the cation, anion, and total diffusion coefficients, using the Vogel temperature (T_0) from the ionic conductivity VFT fits listed in **Table S3**.

	IL			MIC		
Ion	log D_∞ ($m^2 s^{-1}$)	B	T_0 (K)	log D_∞ ($m^2 s^{-1}$)	B	T_0 (K)
BMIm-DCA						
$BMIm^+$	-7.89	5.3	155	-8.18	4.8	161
DCA^-	-7.75	5.3	155	N/A	N/A	N/A
EMIm-TfO						
$EMIm^+$	-8.03	5.0	154	-8.03	6.2	145
TfO^-	-8.05	5.4	154	-8.06	6.7	145
BMIm-TfO						
$BMIm^+$	-7.8	6.0	160	-7.37	13	120
TfO^-	-7.81	6.2	160	-7.38	13	120
EMIm-TFSI						
$EMIm^+$	-7.81	6.0	146	-7.95	5.7	155
$TFSI^-$	-7.90	6.3	146	-8.03	6.1	155
BMIm-TFSI						
$BMIm^+$	-7.83	6.0	152	-8.00	6.4	153
$TFSI^-$	-7.86	6.2	152	-8.05	6.7	153
BMPyr-TFSI						
$BMPyr^+$	-7.78	6.7	151	-7.87	6.6	156
$TFSI^-$	-7.81	6.8	151	-7.94	6.6	156

Normalized Room Temperature MIC Diffusivity

Similar to the ionic conductivity, we compared the differences in the ionic diffusivity between the IL and MIC by normalizing the ionic diffusivity of the MIC (D_{MIC}) with the ionic diffusivity of the IL (D_{IL}) at 30 °C. **Figure S6** shows that the all MICs produce an ionic diffusivity within a factor of 3 of their respective IL, paralleling well with the trends shown in the normalized MIC ionic conductivity (**Figure S4**).

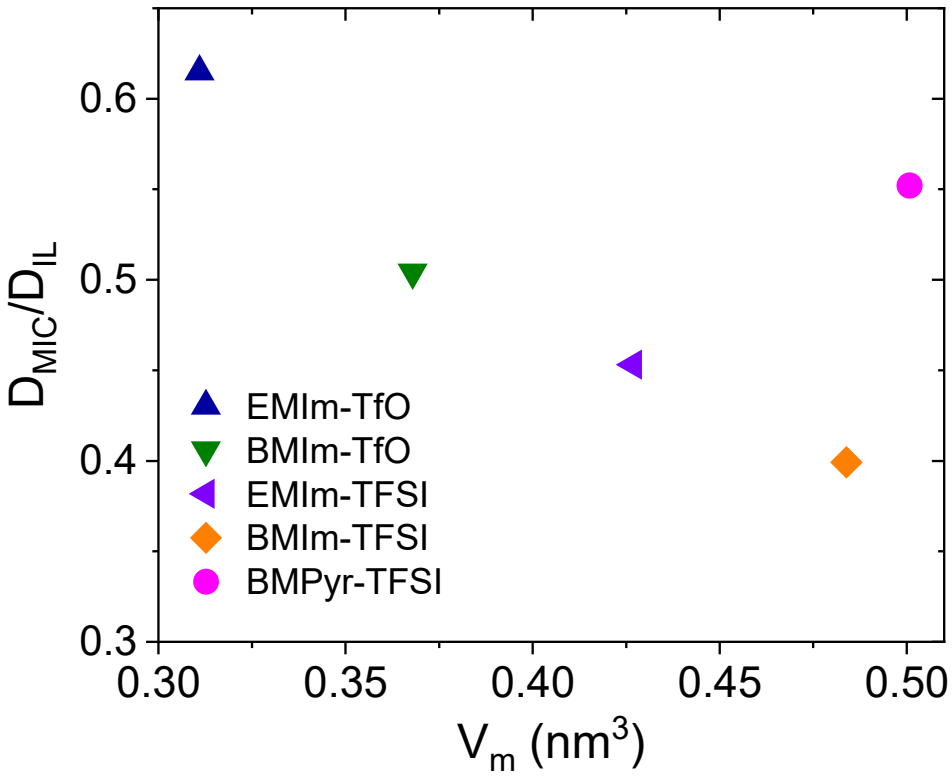

Figure S6: V_m dependence of the normalized MIC diffusivity (D_{MIC}/D_{IL}) at 30 °C. All MICs maintain a diffusivity within roughly a factor of 3 of their respective IL, agreeing well with the normalized MIC ionic conductivity.

References

1. M. Rubinstein and R. H. Colby, *Polymer Physics*, Oxford University Press, New York, 2003.
2. R. J. Fox, D. Yu, M. Hegde, A. S. Kumbhar, L. A. Madsen and T. J. Dingemans, *ACS Applied Materials & Interfaces*, 2019, **11**, 40551-40563.
3. D. Fragiadakis, S. Dou, R. H. Colby and J. Runt, *Journal of Chemical Physics*, 2009, **130**, 064907.
4. D. Fragiadakis, S. Dou, R. H. Colby and J. Runt, *Macromolecules*, 2008, **41**, 5723-5728.
5. M. Wübbenhorst and J. van Turnhout, *Journal of Non-Crystalline Solids*, 2002, **305**, 40-49.
6. U. H. Choi, A. Mittal, T. L. Price, H. W. Gibson, J. Runt and R. H. Colby, *Macromolecules*, 2013, **46**, 1175-1186.
7. S. Havriliak and S. Negami, *Polymer*, 1967, **8**, 161-210.
8. J. R. Sangoro and F. Kremer, *Accounts of Chemical Research*, 2012, **45**, 525-532.
9. C. Krause, J. R. Sangoro, C. Iacob and F. Kremer, *The Journal of Physical Chemistry B*, 2010, **114**, 382-386.
10. J. E. Bostwick, C. J. Zanelotti, C. Iacob, A. G. Korovich, L. A. Madsen and R. H. Colby, *Macromolecules*, 2020, **53**, 1405-1414.
11. F. Kremer and A. Schönhals, *Broadband Dielectric Spectroscopy*, Springer, Berlin, Heidelberg, New York, 2003.